# Chemical Shift MR Imaging of the Adrenal Gland: Principles, Pitfalls, and Applications[1]

*Sharon Z. Adam, MD*
*Paul Nikolaidis, MD*
*Jeanne M. Horowitz, MD*
*Helena Gabriel, MD*
*Nancy A. Hammond, MD*
*Tanvi Patel, MD*
*Vahid Yaghmai, MD*
*Frank H. Miller, MD*

**Abbreviations:** ASII = adrenal signal intensity index, FDG = fluorodeoxyglucose, HART = hepatic adrenal rest tumor, HCC = hepatocellular carcinoma, RCC = renal cell carcinoma, 3D = three-dimensional, 2D = two-dimensional

**RadioGraphics 2016;** 36:0000–0000

**Published online** 10.1148/rg.2016150139

**Content Codes:** CT GU MR OI

[1]From the Department of Radiology, Northwestern Memorial Hospital, Northwestern University Feinberg School of Medicine, 676 N Saint Clair St, Suite 800, Chicago, IL 60611. Presented as an education exhibit at the 2014 RSNA Annual Meeting. Received May 4, 2015; revision requested August 7 and received August 31; accepted September 10. For this journal-based SA-CME activity, the authors, editor, and reviewers have disclosed no relevant relationships. **Address correspondence to** F.H.M. (e-mail: *fmiller@northwestern.edu*).



## SA-CME LEARNING OBJECTIVES

*After completing this journal-based SA-CME activity, participants will be able to:*

- Describe the physics behind chemical shift MR imaging.
- Identify the correct techniques to achieve optimal chemical shift imaging of the adrenal gland and avoid technical pitfalls.
- Discuss clinical applications of chemical shift imaging to diagnosing adrenal lesions.

*See www.rsna.org/education/search/RG.*

Adrenal lesions are a common imaging finding. The vast majority of adrenal lesions are adenomas, which contain intracytoplasmic (microscopic) fat. It is important to distinguish between adenomas and malignant tumors, and chemical shift magnetic resonance (MR) imaging can be used to accomplish this distinction by depicting the fat in adenomas. Chemical shift imaging is based on the difference in precession frequencies of water and fat molecules, which causes them to be in different relative phases during the acquisition sequence and allows in-phase and opposed-phase images to be obtained. It is important to acquire these images by using the earliest possible echo times, with the opposed-phase echo before the in-phase echo, and by using a single breath hold to preserve diagnostic accuracy. Intracytoplasmic fat is depicted as signal drop on opposed-phase images when compared with in-phase images. Both qualitative and quantitative methods for assessing signal drop are detailed. The appearances of adrenal adenomas and other adrenal tumors on chemical shift MR images are described, and discriminatory ability at chemical shift MR imaging compared with that at adrenal computed tomography (CT) is explained. Other adrenal-related conditions in which chemical shift MR imaging is helpful are also discussed. Chemical shift MR imaging is a robust tool for evaluating adrenal lesions that are indeterminate at nonenhanced CT. However, it is important to know the advantages and disadvantages, including several potential imaging pitfalls. The characterization of adrenal lesions by using chemical shift MR imaging and adrenal CT should always occur in the appropriate clinical setting.



## Introduction

Adrenal lesions are a relatively common imaging finding, and most are incidentalomas that are detected at imaging performed for other reasons. Adrenal incidentalomas are seen in 1%–4.2% of the population. They have become a more frequent finding as use of imaging has increased over the past few decades (1–3). Most adrenal lesions are benign and clinically unimportant (1,4). The vast majority are adenomas (1), lesions that contain a high percentage of intracytoplasmic lipids, which should allow their diagnosis at nonenhanced computed tomography (CT) and magnetic resonance (MR) imaging (5,6). It is important to distinguish adrenal adenomas from malignant adrenal lesions. This is especially crucial in patients with a primary malignancy elsewhere, in whom only 26%–36% of adrenal nodules are metastatic (7), because diagnosis of an adrenal metastasis will lead to altered treatment and prognosis.

Although CT is well established for characterizing adrenal incidentalomas as adenomas because of their nonenhanced appearance and washout profile, MR imaging also is a valuable modality for characterizing adrenal incidentalomas. The growing use of abdominal MR

## TEACHING POINTS

- When the protons are in the same location (in phase), the signals received from fat and water protons in the same voxel are additive. When they are in completely opposing phases (opposed phase), the signals cancel each other out. This causes signal drop on opposed-phased images in tissues that contain microscopic fat, which appear darker than they did on in-phase images.
- The end result of a Dixon sequence is four sets of images: water-only, fat-only, in-phase, and opposed-phase. This method allows the radiologist to quantify microscopic fat in addition to detecting its presence.
- The longer the echo time, the more T2* decay will reduce signal intensity, making it more difficult to interpret the signal drop expected from microscopic fat and potentially compromising diagnostic accuracy. For this reason, the shortest echo times feasible should be chosen.
- To minimize the effect of T2* decay on opposed-phase images, the opposed-phase echo must always be acquired before the in-phase echo to prevent overlap between adenomas and other lesions.
- Indeterminate lesions seen at nonenhanced CT may be further evaluated by using either contrast-enhanced CT with an adrenal protocol, which can depict contrast washout characteristics typical of an adenoma, or chemical shift MR imaging, which can depict lipid in lesions that are described as lipid-poor at nonenhanced CT (ie, attenuation higher than 10 HU) but are seen to contain an abundance of lipid at MR imaging (by demonstrating signal drop on opposed-phase images).

imaging for other indications has resulted in an increasing number of adrenal incidentalomas that are detected at MR imaging rather than at CT. Therefore, understanding the MR techniques used in adrenal imaging is important.

This article clarifies the pathologic and physical principles behind chemical shift imaging, explains proper techniques for performing chemical shift imaging and the potential technical pitfalls, and describes clinical applications of chemical shift imaging to the adrenal gland.

## Principles of Chemical Shift Imaging

### Pathologic Basis for Imaging

The distinguishing feature of most adrenal adenomas is a high content of intracytoplasmic lipids, which are precursors of adrenal hormone production (4,5) and are visible microscopically. Routine fat-suppressed MR imaging techniques, such as inversion-recovery or frequency-selective fat-suppression sequences, can be used to depict fat that is macroscopically visible (8) but not the microscopic intracytoplasmic fat in adenomas. However, chemical shift imaging can be used to depict microscopic amounts of intracytoplasmic fat (9), which makes it useful for characterization of adrenal adenomas. Because distinguishing between adenomas and other adrenal lesions is the main goal of adrenal imaging, chemical shift imaging is the mainstay of adrenal MR imaging.

### Chemical Shift Physics

Chemical shift imaging is based on innate differences in the inherent magnetic field experienced by the protons in fat molecules compared with those in water molecules, which are caused by the effects of the nonproton components of the molecules (carbon vs oxygen, respectively) on the electron cloud that surrounds the protons (8). This weak magnetic field opposes the external magnetic field caused by the MR imaging unit, a phenomenon called shielding, and is also proportional to the external magnetic field. The shielding effect is stronger in fat molecules than in water molecules, causing the protons in fat to experience a lower effective magnetic field.

A basic principle of MR imaging is that protons precess in a specific frequency when placed in a magnetic field. The precession frequency is determined by the effective magnetic field. The difference in the effective magnetic field causes a different precession frequency for fat and water protons. Because the effective magnetic field is dependent on the external magnetic field, the differences in precession frequency are also dependent on the external magnetic field and are usually considered to be 225 Hz at 1.5 T and 450 Hz at 3 T. However, because this phenomenon depends on the structure of the molecule and its environment, it is also affected by outside conditions, such as pH level, temperature, and the specific fat molecule structure (which can be heterogeneous) (10). These conditions cause variations in the frequency difference, which has been reported to range from 210 to 225 Hz at 1.5 T and from 420 to 450 Hz at 3 T (8,11,12). The same chemical principle is valid for protons in any molecule; hence the term *chemical shift*. Chemical shift is calculated by dividing the frequency difference between the protons by the Larmor frequency of the outside magnet (ie, the MR imaging unit), and it is a dimensionless number reported in parts per million. For fat and water, the chemical shift is 3.3–3.5 ppm (Fig 1).

## Techniques and Technical Pitfalls

Chemical shift imaging, also known as in-phase and opposed-phase imaging, includes traditional acquisitions of in-phase and opposed-phase images and use of the newer Dixon method and its modifications.

In-phase and opposed-phase imaging is based on the phase-cancellation artifact caused by chemical shift, also known as type 2 chemical shift artifact

$$\delta = \frac{\Delta f}{\omega_0} = \frac{\Delta f}{\gamma B_0}$$

$$\Delta f = \delta \times \omega_0 = \delta \times \gamma B_0$$

$$\Delta f = 3.5 \times 63.75 = 3.5 \times 42.5 \times 1.5 = 223.125 \text{Hz}$$

**Figure 1.** Mathematical representations show the relationship between the chemical shift of fat and water (δ, in parts per million), the difference in precession frequency of fat and water (Δ*f*, in hertz), and the Larmor frequency of the MR imaging unit ($\omega_0$, in megahertz). The Larmor frequency is dependent on the external magnetic field ($B_0$, in tesla) and the gyromagnetic ratio of protons (γ, in radians per second per tesla). Using the most widely used chemical shift of 3.5 ppm, the difference in frequencies between fat and water at 1.5 T is approximately 223 Hz, as shown in the third equation.

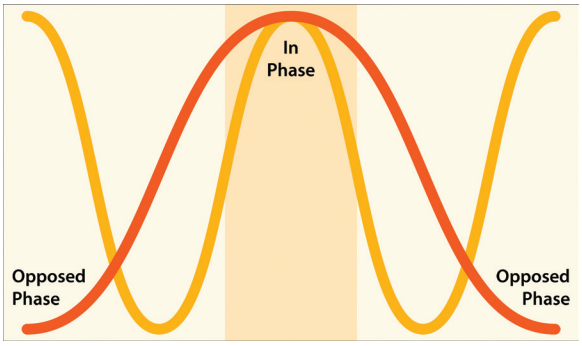


**Figure 2.** Wave illustration of phase versus time for two precession frequencies representing the lower frequency of fat (orange curve) compared with water (yellow curve). The two waves cyclically intersect at certain time points that represent the relative phase of the two frequencies.

(8). The different precession frequencies of fat and water protons cause them to be in the same longitudinal location at only set times during the precession cycle, while being at different degrees of out of phase at all other times (Fig 2). When the protons are in the same location (in phase), the signals received from protons of fat and water in the same voxel are additive. When they are in completely opposing phases (opposed phase), the signals cancel each other out. This causes signal drop on opposed-phase images in tissues that contain microscopic fat, which appear darker than they did on in-phase images. This is a cyclic process: protons start in phase and then are in phase every 1/frequency difference and are perfectly in opposed phase every half of that time. This time is, in effect, the echo time. At 1.5 T, the phase shift from in phase to opposed phase occurs every 2.2 msec, and at 3 T it occurs every 1.1 msec (13). Traditional in-phase and opposed-phase imaging is performed by using gradient-recalled sequences. All sequence parameters must be identical except for echo time. Currently, this technique is usually performed by using a dual-echo sequence rather than separate acquisitions; therefore, variability in other parameters is not a concern.

The Dixon method and its modifications are based on a similar principle of acquiring in-phase and opposed-phase images and then using a mathematical calculation in postprocessing to create images containing water-only signal and fat-only signal. The original Dixon method used two time points, assuming a single fat proton frequency just like traditional in-phase and opposed-phase imaging, but its modifications can take into account three or more time points along the phase shift cycle to account for the variable frequencies of fat protons. Dixon methods can be performed by using gradient-recalled-echo, spin-echo, or steady-state free precession sequences, and a multiecho single acquisition is used for both in-phase and opposed-phase data. The end result of a Dixon sequence is four sets of images: water-only, fat-only, in-phase, and opposed-phase. This method allows the radiologist to quantify microscopic fat in addition to detecting its presence. A problem unique to this method is fat-water swapping. This can occur when magnetic field inhomogeneities cause a miscalculation that results in fat being detected as water and vice versa (14). When this occurs, the fat-only and water-only images are unreliable, and only the in-phase and opposed-phase images can be used, similar to traditional in-phase and opposed-phase imaging.

An artifact appears on opposed-phase images, regardless of the acquisition method, that causes the abdominal organs to be delineated by a dark line wherever the organs interface with abdominal fat (11). This is caused by the coexistence of fat and water in the interfacing voxel, which leads to signal cancellation. This artifact is known as etching artifact, "India ink" artifact, or black boundary artifact (Fig 3). It allows quick identification of an opposed-phase image and can sometimes aid in diagnosis but may also lead to interpretation pitfalls, as will be explained later.

## T2* Decay and Echo Timing

Choosing the echo time correctly is important for reducing the effects of T2* decay on signal intensity. The longer the echo time, the more T2* decay will reduce signal intensity, making it more difficult to interpret the signal drop expected from microscopic fat and potentially compromising diagnostic accuracy (15). For this reason, the shortest echo times feasible should be chosen.

Minimizing the effect of T2* decay is more important on opposed-phase images than on in-phase images because the goal is to assess signal drop on opposed-phase images, which may be confounded by signal drop caused by T2* decay. Because in-phase images are used only as a reference for signal drop, T2* decay is of less concern

**Figure 3.** Typical adrenal adenoma in a 55-year-old woman. The lesion was incidentally discovered at abdominal CT performed for abdominal pain, which demonstrated a 1.7-cm indeterminate left adrenal lesion. Chemical shift MR imaging was performed for characterization by using the Dixon method. Axial in-phase **(a)** and opposed-phase **(b)** images show lower signal intensity in the lesion (arrow) on the opposed-phase image compared with the in-phase image. The lesion has high signal intensity on a corresponding fat-only image **(c)** and intermediate-low signal intensity on a water-only image **(d)**. It appears bright on a subtraction image **(e)**, which further proves the presence of signal drop. Note the etching ("India ink") artifact on the opposed-phase image in **b**, seen as a black line separating the abdominal organs from intra-abdominal fat. The findings prove the presence of intracytoplasmic fat, indicative of an adenoma.

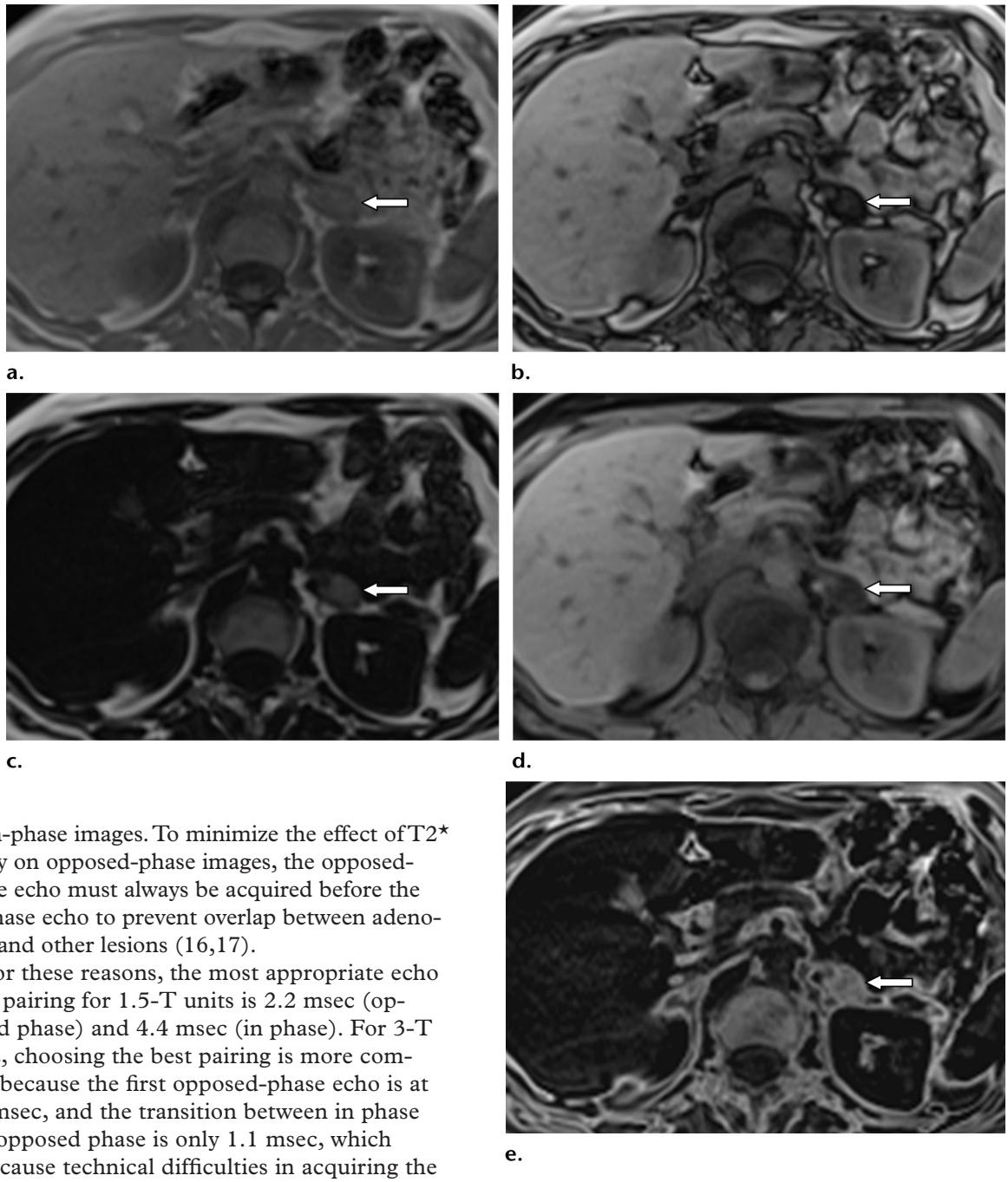


on in-phase images. To minimize the effect of T2* decay on opposed-phase images, the opposed-phase echo must always be acquired before the in-phase echo to prevent overlap between adenomas and other lesions (16,17).

For these reasons, the most appropriate echo time pairing for 1.5-T units is 2.2 msec (opposed phase) and 4.4 msec (in phase). For 3-T units, choosing the best pairing is more complex because the first opposed-phase echo is at 1.1 msec, and the transition between in phase and opposed phase is only 1.1 msec, which may cause technical difficulties in acquiring the 1.1- and 2.2-msec pair. Increasing the receiver bandwidth and using parallel imaging can help reduce imaging time and allow use of the 1.1- and 2.2-msec pair, at the cost of reduced signal-to-noise ratio. When this yields unacceptable image quality, one may use the first opposed-phase echo and the second in-phase echo (1.1 and 4.4 msec) or choose the second echo pair (3.3 and 4.4 msec) (17). This is not a concern when images are acquired with a multiecho single-acquisition Dixon method.

## Acquiring Echo-Pair Images in the Same Breath Hold

Opposed-phase and in-phase images should be acquired by using a single breath hold. Performing

**Table 1: Quantitative Signal Drop Calculation Methods and Suggested Cutoff Values for Adenomas, as Recently Reported in the Literature**

| Name | Formula | Cutoff Value at 1.5 T | Cutoff Value at 3 T |
|---|---|---|---|
| Adrenal signal intensity index (ASII)* | $\frac{\text{(lesion IP)} - \text{(lesion OP)}}{\text{(lesion IP)}} \cdot 100$ | >16.5% | >1.7% |
| Adrenal-to-spleen ratio (ASR)† | $\left[\frac{\text{(lesion OP)/(spleen OP)}}{\text{(lesion IP)/(spleen IP)}} - 1\right] \cdot 100$ | ≤−35.9% | ≤−17.2% |
| Adrenal-to-liver ratio (ALR)† | $\left[\frac{\text{(lesion OP)/(liver OP)}}{\text{(lesion IP)/(liver IP)}} - 1\right] \cdot 100$ | ≤−32.6% | ≤−24.5% |
| Adrenal-to-muscle ratio (AMR)† | $\left[\frac{\text{(lesion OP)/(muscle OP)}}{\text{(lesion IP)/(muscle IP)}} - 1\right] \cdot 100$ | ≤−29.3% | ≤−39.6% |

Note.—For ASR, ALR, and AMR, percentages and decimals are used interchangeably in the literature, and while some authors use the ratio to describe the signal loss, others use the same terminology to describe the signal remaining in the lesion. We report all ratios by using percentages of signal loss for uniformity, as reported in recent literature. IP = in phase, OP = out of phase.
*Data are from reference 17.
†Data are from reference 22.

the two phases in different breath holds may enable use of the first echo pair on 3-T units, but at a cost of reduced quantitative ability and misregistration of images that limits subtraction analysis (15), which is usually diagnostically unacceptable.

If other options fail to achieve acceptable image quality by using the desired echo pairs and it is necessary to acquire in-phase and opposed-phase images in separate breath holds, a two-dimensional (2D) acquisition sequence is preferred over a three-dimensional (3D) sequence because 2D acquisition is less sensitive to motion artifacts and therefore less likely to cause misregistration. In these cases, care must be taken when calculating signal drop because the reference values for adrenal lesions differ between 3D and 2D acquisition (as will be discussed in the "Image Analysis" section) (18,19).

### Accuracy of Echo Times

Adherence to exact echo times is crucial with 3-T units compared with 1.5-T units. On 1.5-T units, very small time drifts from ideal in-phase and opposed-phase times are acceptable. However, on 3-T units, these small drifts from the ideal timing are unacceptable because any time drift is relative to the transition between in phase and opposed phase, which is twice as rapid on 3-T units (15). Such drifts can therefore create an altered signal change between the phases, causing diagnostic inaccuracies.

## Image Analysis

Traditional in-phase and opposed-phase imaging is more widely used for evaluating adrenal lesions than is measurement of fat percentage with the Dixon method. Both qualitative and quantitative methods exist for assessing the presence of fat in a lesion on traditional in-phase and opposed-phase images.

Qualitative assessment is composed of visual assessment of opposed-phase images compared with in-phase images to evaluate for signal drop, using adjacent structures that are visible on the same section as a visual reference (eg, the liver and spleen). This method is the most widely used, probably because it is not time consuming, and is considered as reliable as quantitative analysis (20–22). Subtraction images can be created by subtracting opposed-phase signal from in-phase signal for every voxel. The result is an image on which tissues with signal drop (ie, microscopic fat) appear bright, as opposed to all other tissues, which are virtually black (Fig 3). Subtraction images can increase readers' confidence in visual evaluation of signal drop (23), especially when there is signal drop in the liver due to fatty infiltration.

Quantitative analysis entails drawing regions of interest on the lesion on both in-phase and opposed-phase images and then calculating signal drop. The various calculation methods are detailed in Table 1. The simplest way is to determine the percentage of signal drop relative to the lesion's signal intensity on the in-phase images. This is referred to as the ASII. Signal intensity is affected by sequence parameters, and the different techniques used in different centers can cause differences in absolute values. Therefore, some formulas use a "normalized" signal intensity value by using a reference tissue. These formulas calculate the ratio between signal intensity on opposed-phase and in-phase images in relation to a reference tissue. Most studies use the liver, spleen, or paraspinal muscles as a

reference (17,22). The spleen is the most commonly used reference tissue because the liver and muscles may be unreliable because of fatty infiltration. Less commonly, the spleen may be unreliable because of iron deposition, in which case the kidney can be used as a reference (24). The same principles for choosing the reference tissue apply to qualitative assessment. Of note, field strength affects the result of these calculations, and therefore signal drop cutoff values for distinguishing adenomas from other lesions differ between 1.5-T and 3-T units (22).

With use of the Dixon method, measurement of the fat content of a lesion can be accomplished in addition to using the aforementioned calculations on in-phase and opposed-phase images. Two quantitative parameters, fat fraction and fat ratio, have been used. *Fat fraction* is the signal intensity of a lesion as measured on the fat-only image, divided by the sum of signal intensities on the fat-only and water-only images. *Fat ratio* is the signal intensity of a lesion as measured on the fat-only image, divided by the signal intensity of subcutaneous fat in the anterior abdominal wall. The fat fraction is considered more reliable because it uses a single region of interest that is placed in the same location on all images (25).

## Clinical Applications

Adrenal adenoma is the most common adrenal lesion and is estimated to exist in 1.4%–8.9% of the population (26). Nodular hyperplasia, myelolipomas, cysts or pseudocysts, hemorrhage (secondary to trauma, anticoagulation therapy, or hypertension), pheochromocytomas, adrenocortical carcinomas, and metastases are less commonly seen. Other benign and malignant lesions can occur in the adrenal glands (eg, lipoma, ganglioneuroma, hamartoma, hemangioma, angiomyolipoma, neurofibroma, lymphoma, and neuroblastoma) but are extremely rare (1,26).

The main focus of adrenal imaging is distinguishing between adenomatous and nonadenomatous lesions to determine which lesions may be suspicious for malignancy and require further evaluation (15). Adenomas with a high lipid content can be distinguished reliably from other lesions on the basis of *(a)* signal drop at chemical shift MR imaging, which is caused by intracytoplasmic lipid, *(b)* low attenuation from fat at nonenhanced CT, and *(c)* contrast material washout characteristics at CT. While chemical shift MR imaging and adrenal CT offer high sensitivity and specificity for diagnosis of adenomas, it is important to note that adrenal lesions that do not meet strict CT washout or chemical shift MR imaging criteria for adenomas have a wide differential diagnosis. Although these lesions may be "lipid-poor" adenomas, other benign and malignant causes must be considered in the differential diagnosis (26). Rarely, some malignant tumors may mimic adenomas at both CT and chemical shift MR imaging but can often be differentiated on the basis of clinical history and other findings.

### Adrenal Adenomas

Adenomas are typically designated as either lipid-rich or lipid-poor based on their appearance at nonenhanced CT. The abundance of intracytoplasmic lipids seen in most adenomas corresponds to low attenuation seen at nonenhanced CT (4,27), which designates them as lipid-rich adenomas. The accepted cutoff value for this diagnosis at nonenhanced CT is 10 HU, which corresponds to a sensitivity of 71% and a specificity of 98% (28). Therefore, attenuation below 10 HU at nonenhanced CT should be considered diagnostic of an adenoma, regardless of the enhancement and washout pattern (29). Lipid-poor adenomas, which account for 10%–40% of all adenomas, are those that have a higher attenuation at nonenhanced CT and are therefore considered indeterminate and require further imaging for characterization. With the growing use of dual-energy CT, it should be noted that the attenuation of adenomas on virtual nonenhanced images can be used reliably for diagnosis (30) (Fig 4), although this attenuation may be higher than on true nonenhanced images (31). Therefore, use of a 10-HU cutoff value on virtual nonenhanced images is safe for diagnosis of adenomas but may lead to a higher rate of indeterminate lesions than with true nonenhanced images (31). Material analysis at dual-energy CT is also showing promise, and a recent study has shown its superiority over nonenhanced CT for diagnosis of adenomas (32).

Indeterminate lesions seen at nonenhanced CT may be further evaluated by using either contrast-enhanced CT with an adrenal protocol, which can depict contrast washout characteristics typical of an adenoma, or chemical shift MR imaging, which can detect lipid in lesions that are described as lipid-poor at nonenhanced CT (ie, those with attenuation higher than 10 HU) but are seen to contain an abundance of lipids at MR imaging (ie, signal drop on opposed-phase images) (9) (Fig 3).

Adrenal adenomas typically demonstrate brisk arterial enhancement and rapid delayed phase washout of contrast material compared with nonadenomatous lesions. When enhancement characteristics of an adrenal lesion are evaluated at CT, the imaging study should ideally include nonenhanced, portal venous (60–75 sec), and delayed (15 min) phases. Studies have shown that calculations that use the arterial phase are less

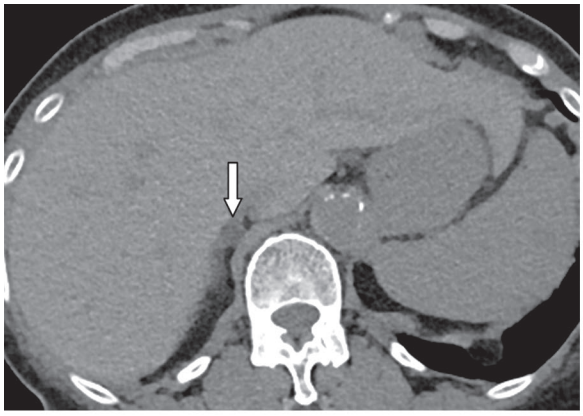

a.

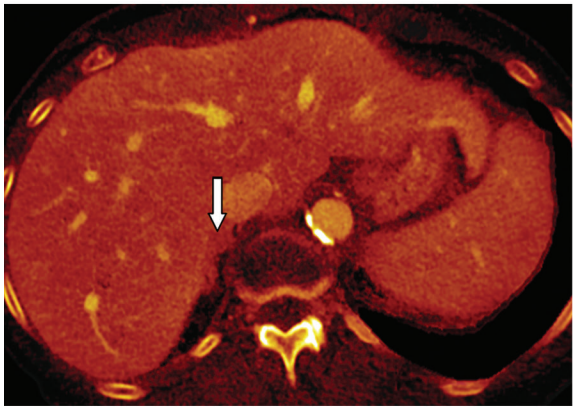

b.

c.

**Figure 4.** Small adrenal adenoma discovered incidentally in an 82-year-old woman undergoing dual-energy triphasic CT for evaluation of hematuria. Axial CT images reveal a small lesion (arrow) measuring 8.3 HU on a true nonenhanced image **(a)**, with iodine uptake seen on a contrast-enhanced image with iodine mapping **(b)** and a corresponding attenuation of 5.6 HU seen on a virtual nonenhanced image **(c)**. The lesion demonstrated an iodine density of 3.0 mg/mL and a fat fraction of 34.5%.

sensitive and less specific than widely used washout calculations (33,34), and arterial phase scans are therefore not recommended as part of routine dedicated adrenal protocols. Washout is calculated at adrenal CT by using two different formulas—absolute washout and relative washout (Table 2). The timing of delayed imaging is important, and different cutoff values have been found for different times. Most studies advocate use of a 15-minute delay, for which the recommended minimal absolute washout value is 60% (corresponding to sensitivity and specificity of 84%–86% and 79%–92%, respectively, for lipid-poor adenomas), and the recommended minimal relative washout value is 40% (corresponding to sensitivity and specificity of 82%–92% and 75%–92%, respectively) (35,36). An important caveat (further described in the following sections) is that some pheochromocytomas, and more rarely metastases from certain hypervascular tumors, may demonstrate intense enhancement and contrast washout, causing washout rates that mimic those of adenomas. Many articles that report extremely high sensitivity and specificity for diagnosing adenomas (eg, 98% and 100%, respectively) at adrenal CT are reporting rates for all adenomas, including lipid-rich adenomas, when in fact the rates for lipid-poor adenomas are lower in most studies.

MR imaging has been gaining favor for adrenal imaging because of CT-related radiation concerns and the usefulness of MR imaging in patients for whom contrast material is contraindicated, along with improvements in the quality and availability of abdominal MR imaging in recent years. A recommended MR imaging protocol for evaluating adrenal lesions is detailed in Table 3. Routine T1- and T2-weighted sequences are not helpful in diagnosing adrenal adenomas (21). MR imaging enhancement patterns have also been studied by several groups, focusing on qualitative and quantitative evaluation of early arterial (8–10 sec after the bolus reaches the celiac trunk), early venous (45–70 sec), and late venous or equilibrium (90–180 sec) phases (37,38). The enhancement patterns typically seen in adenomas are intense arterial blush and, to a lesser extent, mild homogeneous enhancement (37). Other enhancement patterns (patchy, peripheral, punctate, or negligible arterial phase enhancement) used to differentiate adenomas from nonadenomatous lesions showed only 81% sensitivity and 93% specificity, but in combination with chemical shift imaging, these rates improved to 94% and 98%, respectively (while chemical shift imaging alone yielded a sensitivity of 87% and a specificity of 95%) in one study (37). Therefore, the arterial phase

**Table 2: Methods of Calculating Washout at Adrenal CT**

| Factor | Formula or Method |
|---|---|
| Absolute washout percentage | $\frac{Apv - Adel}{Apv - An} \cdot 100$ |
| Relative washout percentage | $\frac{Apv - Adel}{Apv} \cdot 100$ |
| ROI size and placement | ROI size: at least half the size of the lesion; ROI placement: avoid regions of hemorrhage, necrosis, and calcifications and the edges of the lesion |

Source.—References 29 and 35.
Note.—*Adel* = attenuation in delayed phase, *Apv* = attenuation in portal venous phase, *An* = attenuation in nonenhanced phase, ROI = region of interest.

**Table 3: Suggested Protocol for Adrenal MR Imaging**

| Sequence Type | Imaging Plane | Section Thickness (mm) |
|---|---|---|
| T2-weighted | Axial and coronal | 5 |
| T1-weighted gradient-echo in-phase and opposed-phase | Axial and coronal | 3 |
| T1-weighted fat-suppressed gradient-echo | Axial | 3 |
| Optional sequence: diffusion-weighted (*b* values of 50, 500, and 800 sec/mm$^2$) | Axial | 6 |
| Optional sequence: T1-weighted fat-suppressed gradient-echo dynamic contrast-enhanced | Axial and coronal | 3 |

enhancement pattern has been reported as helpful in assessing lesions with indeterminate findings at chemical shift imaging (37). Time to maximal enhancement has also been suggested as a means of diagnosing adenomas (39), reaching moderate sensitivity and specificity of 88% and 80%, respectively, when using 52.85 seconds as the cutoff. Washout characteristics at MR imaging have scarcely been studied. Only two studies used delayed phase imaging equivalent to the timing used at CT (at least 10 minutes after contrast agent administration) (21,40), with conflicting results, although it is unclear whether a long time delay is necessary at MR imaging. One study found no discriminatory ability (21), while the other found a sensitivity of 92% and a specificity of 90% (40).

Chemical shift imaging has been shown to be the best MR imaging technique for adenoma characterization (41). When an adrenal lesion is detected incidentally at MR imaging performed for other reasons, chemical shift imaging can be used to make an immediate diagnosis of adenoma and should be included in every abdominal MR imaging protocol. Chemical shift sequences add approximately 1 minute to the imaging time and do not substantially decrease patient throughput. When performing dedicated MR imaging for a suspected adrenal lesion, we recommend that not only routine axial chemical shift sequences be performed, but also coronal chemical shift sequences, which can be helpful to clarify the organ of origin in difficult cases and allow increased certainty of signal drop (especially when one plane is limited by artifacts). The reported sensitivity and specificity of chemical shift imaging in indeterminate lesions are 67% and 89%–100%, respectively (24,36). Subgroup analysis reveals that for lesions measuring 10–30 HU, the sensitivity is 89%, which is comparable and potentially better than the data reported for washout CT. However, for lesions measuring more than 30 HU, the sensitivity is only 13%, which means that MR imaging is also not a reliable tool for these lesions, although the specificity can be as high as 100% (24) (Fig 5). Therefore, lesions measuring 10–30 HU can be further evaluated with washout CT or chemical shift MR imaging according to personal and institutional preference, and lesions more than 30 HU are best imaged with washout CT.

Chemical shift cutoff values for distinguishing adrenal adenomas from other tumors vary between different field strengths, and studies have also reported different cutoff values for the same field strength. More data exist for 1.5-T units than for 3-T units; therefore, cutoff values using 1.5-T units are more established (although variations still exist between authors), and most studies use 16.5% for the ASII and 71% for the adrenal-to-spleen ratio. Suggestions have been made by different authors for cutoff values at 3 T,

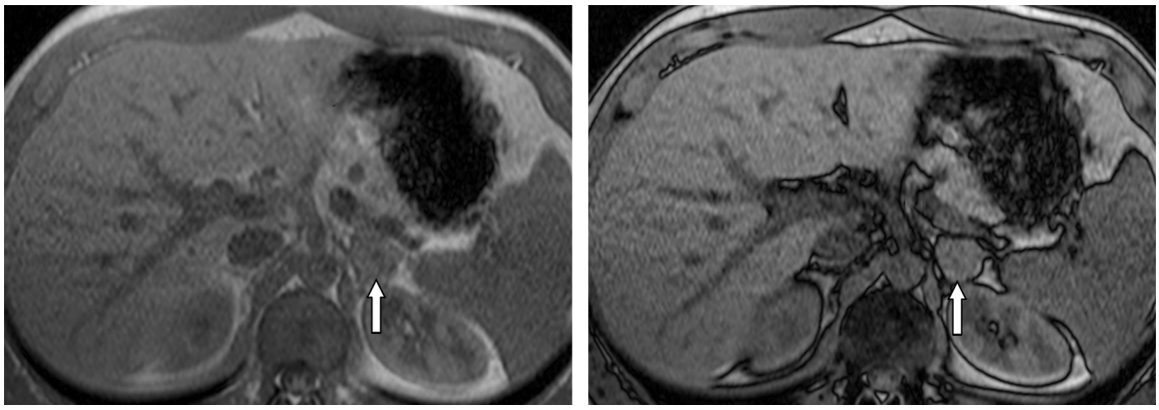

a. b.

**Figure 5.** Adrenal adenoma in a 30-year-old man that was incidentally detected at CT for evaluation of renal colic. CT images (not shown) demonstrated a 2.6-cm lesion in the left adrenal gland, measuring 40 HU, and MR imaging was performed to evaluate this indeterminate lesion. Qualitative analysis of axial in-phase **(a)** and opposed-phase **(b)** MR images showed no signal drop in the lesion (arrow). Quantitative analysis with ASII showed an 11.7% reduction in signal, which does not meet the criteria for adenoma. Findings at adrenal CT with a 15-minute delayed phase (not shown; absolute washout rate, 67.3%; relative washout rate, 49.3%) and stability of the finding after 3 years proved the lesion to be an adenoma that was lipid-poor at CT and MR imaging.

but it is uncertain which values are optimal. Table 1 shows a compilation of recently suggested cutoff values at 1.5 T and 3 T (17,18,22,24).

Use of the Dixon method has not been sufficiently studied for evaluation of adrenal lesions. Only one study has been published (25), which was performed on a 3-T unit and compared three quantitative parameters derived from Dixon sequences (ASII, fat fraction, and fat ratio) without comparing them to traditional in-phase and opposed-phase images. It found no statistically significant differences among the three calculations. ASII had a sensitivity and a specificity of 80% and 93%, respectively, with 23% used as the cutoff value. The sensitivity and specificity of fat fraction were 86% and 82%, respectively, using 16% as the cutoff value, and those of fat ratio were 78% and 86%, respectively, using a 9% cutoff value.

The typical appearance of adrenal adenomas at chemical shift imaging is homogeneous signal drop on opposed-phase images. However, an atypical appearance can occur (42) that is attributed to heterogeneous distribution of lipid-poor and lipid-rich cells within the adenoma (Fig 6). Degenerating adenomas also can have an atypical appearance, such as a large tumor with calcifications and hemorrhage, and may contain little or no microscopic fat, thus mimicking the appearance of more aggressive tumors (Fig 7) (26,43). Therefore, a lesion without signal drop at chemical shift imaging and without typical washout characteristics may still be an adenoma but requires histologic proof.

Diffusion-weighted imaging has been shown to be unreliable for adenoma diagnosis. Diffusion-weighted imaging cannot be used to differentiate lipid-rich from lipid-poor adenomas or to distinguish adenomas from pheochromocytomas, adrenocortical carcinomas, or metastases because significant overlap exists between the apparent diffusion coefficients of adenomas and other adrenal lesions (41,44–46).

Although not used as the first line of imaging for differentiating adrenal adenomas from malignant lesions, positron emission tomography (PET)/CT can be used as a complementary test in difficult cases that remain indeterminate after CT and MR imaging. This is especially true in patients with a known malignancy, who often undergo PET/CT as part of their routine workup. The most commonly used tracer, fluorodeoxyglucose (FDG), can help differentiate benign from malignant adrenal lesions with 74%–100% sensitivity and 66%–100% specificity in oncology patients and has a similar performance in nononcology patients (47). However, false-negative results can occur in lesions less than 8 mm in diameter, malignancies with low FDG avidity, tumor necrosis, and lesions treated with chemotherapy, and false-positive results can occur in certain adenomas and benign pheochromocytomas (47). There is no agreed-on method or threshold for diagnosis of malignancy. Studies have used qualitative assessment of uptake compared with that of background or liver and various quantitative methods such as standardized uptake maximum value (with thresholds ranging from 2.3 to 3.4) and adrenal-to-liver standard uptake value ratio (with thresholds of 1.0 to 2.5) (47).

## Pheochromocytoma

Pheochromocytomas originate in the chromaffin cells of the adrenal medulla (unlike adenomas

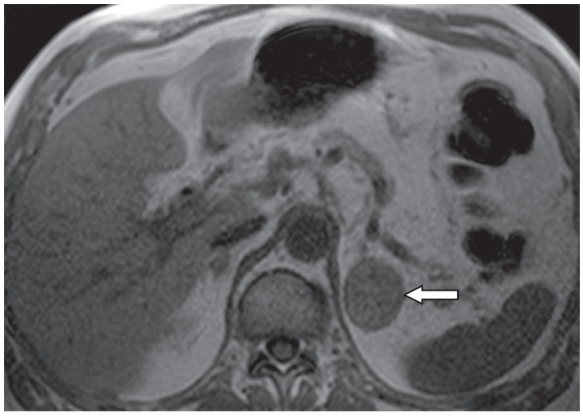

a.

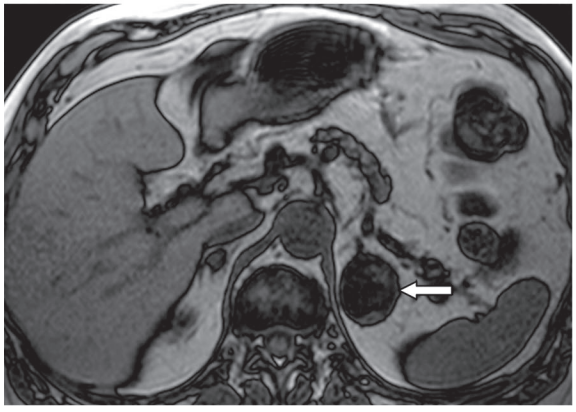

b.

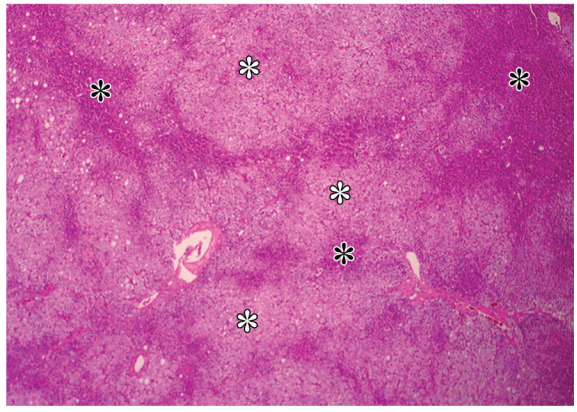

c.

**Figure 6.** Atypical appearances of adrenal lesions. **(a, b)** Axial in-phase **(a)** and opposed-phase **(b)** MR images in an 83-year-old man show an incidentally discovered 4.1-cm lesion in the left adrenal gland (arrow), with markedly heterogeneous signal drop on the opposed-phase image. The finding is consistent with an adenoma that has both lipid-rich and lipid-poor cells. **(c)** Photomicrograph in a different patient shows an adenoma with both lipid-rich (white ∗) and lipid-poor (black ∗) cells. (Hematoxylin-eosin stain; original magnification, ×40.)

and adrenocortical carcinomas, which arise in the cortex) and are the intra-adrenal counterpart of paragangliomas (26). They usually are benign but may be malignant in 10% of cases. They typically secrete catecholamines and therefore often are symptomatic, but asymptomatic tumors are increasing in incidence as incidentalomas are being detected more frequently (26).

Diagnosis of pheochromocytomas at imaging is complex and frequently impossible because they often undergo necrosis, fibrosis, cystic and fatty degeneration, and calcification (48). The typical bright "lightbulb" appearance at T2-weighted MR imaging is actually seen in only 10% of pheochromocytomas (49), and many have a nonspecific appearance (Fig 8).

While nearly all pheochromocytomas do not demonstrate signal drop at chemical shift imaging, fatty degeneration may result in microscopic fat that can cause signal drop and mimic findings of an adenoma (48). Fatty degeneration usually occurs in only a small portion of the lesion, causing minimal signal drop on opposed-phase images (Fig 9), unlike a typical adenoma, in which there is more extensive and uniform signal drop. Profound fatty degeneration leading to large amounts of macroscopic fat may mimic findings of myelolipoma. Pheochromocytomas may mimic adenomas at nonenhanced CT as well because fatty and cystic degeneration may cause low attenuation (50). In some of these cases, MR imaging can aid in correct diagnosis because its superior contrast resolution may better demonstrate the cystic portions of the lesion (Fig 10). The enhancement characteristics of pheochromocytomas may also rarely coincide with those of adenomas. Pheochromocytomas typically enhance avidly, but lack of enhancement can be seen in regions of cystic change or degeneration (48). Heterogeneous enhancement is slightly more common than homogeneous enhancement (52). Some pheochromocytomas may demonstrate contrast washout, with relative or absolute washout rates that mimic those of adenomas (53). This was recently shown to occur in as many as 33% of pheochromocytomas when a 15-minute delay was used (52). However, the overall rarity of pheochromocytomas makes this a rare occurrence in clinical practice.

Despite these possible rare features, other MR imaging findings such as size, heterogeneity, and T2-weighted appearance, along with elevated levels of serum and urine catecholamines, usually enable correct diagnosis. A lesion suspected to be a pheochromocytoma on the basis of MR imaging findings or biochemical

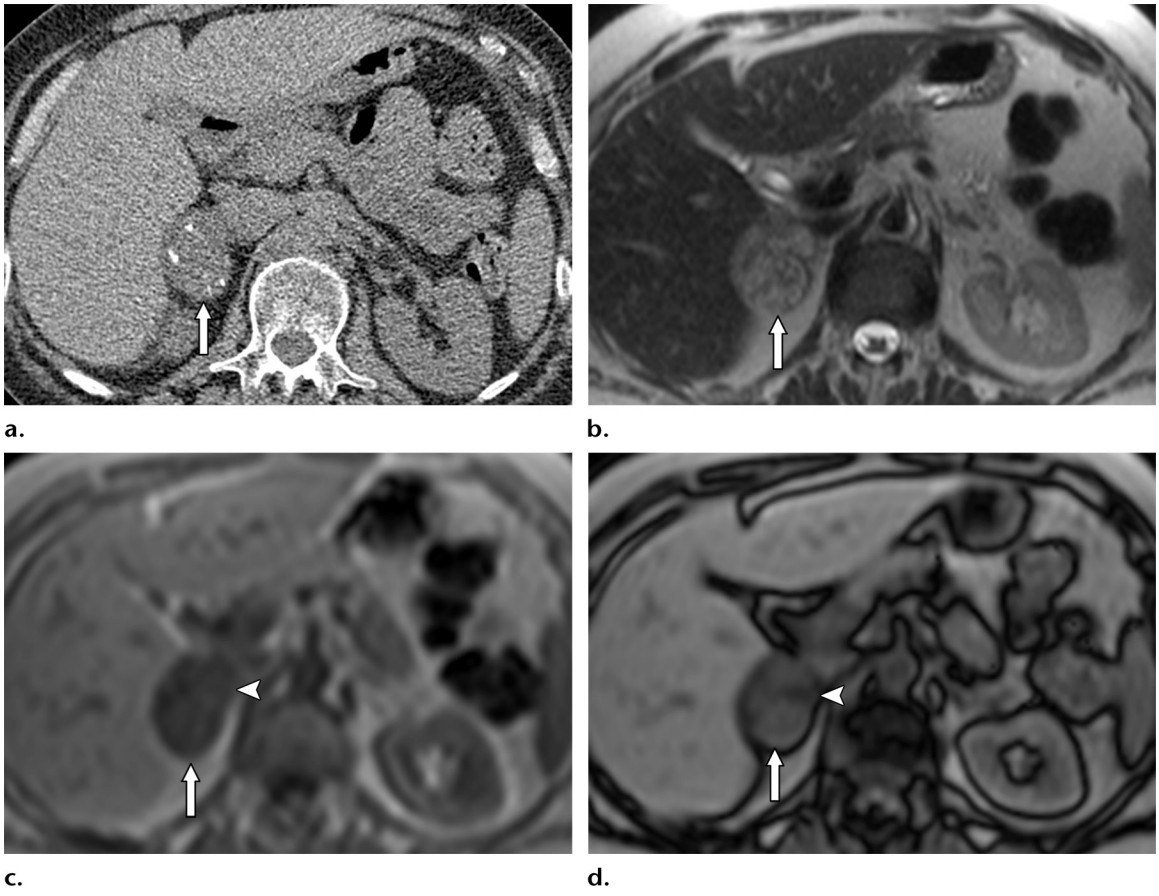


**Figure 7.** Degenerating adenoma incidentally detected in a 62-year-old woman undergoing screening for lung cancer. **(a)** Nonenhanced CT image shows an indeterminate 4.2-cm right adrenal mass (arrow) containing calcifications, with an attenuation of 22 HU. **(b)** Axial T2-weighted MR image shows heterogeneous signal intensity in the mass (arrow). **(c, d)** Comparison of axial in-phase **(c)** and opposed-phase **(d)** MR images shows signal drop in only a small portion of the lesion (arrowhead), while most of the lesion does not show signal drop (arrow). The appearance mimics that of a more aggressive tumor. Histologic analysis after an adrenalectomy demonstrated a partially infarcted adenoma with hemorrhage and calcifications.

activity should be further evaluated with labeled metaiodobenzylguanidine (MIBG) scintigraphy. MIBG scintigraphy also is useful in asymptomatic patients without documented biochemical activity (54); therefore, it cannot be used to distinguish between functioning and nonfunctioning pheochromocytomas. The role of biopsy in these patients is controversial because of the limited yield of biopsy in adrenal incidentalomas in patients without a known malignancy and the added risk for hypertensive complications in these patients (55–57).

## Adrenocortical Carcinoma

Adrenocortical carcinomas are aggressive tumors. They are usually large (9.8 cm on average at resection) and may be functional or nonfunctional (26,58). They may be partially necrotic, hemorrhagic, or calcified and typically invade adjacent structures, often the renal veins and inferior vena cava.

The imaging appearance of adrenocortical carcinomas, including their enhancement patterns and heterogeneous signal intensity at MR imaging, is nonspecific. Very rarely, adrenocortical carcinomas exhibit focal fatty degeneration. These small foci of microscopic fat can show signal drop at chemical shift imaging (59) and may mimic findings of an atypical adrenal adenoma. Fatty degeneration may even lead to foci of macroscopic fat, mimicking the appearance of myelolipomas (60). However, the large size, aggressive appearance and invasiveness, and presence of only small foci of fat should almost always lead to correct diagnosis. Biopsy of suspected adrenocortical carcinomas is usually not encouraged because of the high likelihood of false-negative results (more common in fine-needle aspiration than in core biopsy) leading to misdiagnosis of carcinoma as adenoma and the potential for tumor seeding (55,56). Lesions with suspicious characteristics are usually excised surgically.

## Metastases

Metastases are the most common malignant tumor seen in the adrenal glands. In patients without a known history of malignancy, only 2% of adrenal

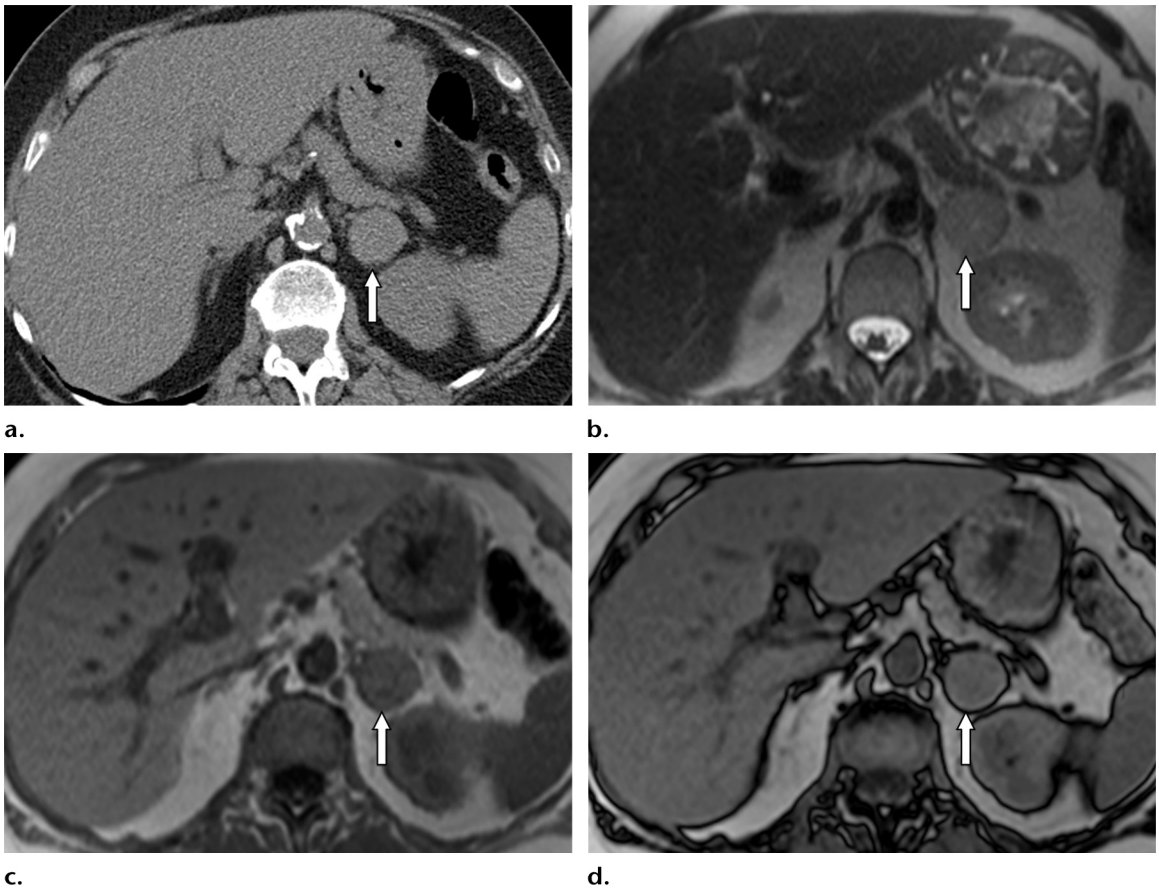


**Figure 8.** Nonspecific appearance of a pheochromocytoma at CT and MR imaging in a 72-year-old woman. The lesion was incidentally found at lower extremity CT angiography. **(a)** Axial nonenhanced CT image shows an indeterminate 2.8-cm lesion in the left adrenal gland (arrow). **(b–d)** Axial T2-weighted **(b)**, in-phase **(c)**, and opposed-phase **(d)** MR images show a mildly T2 hyperintense lesion (arrow) that does not exhibit signal drop on the opposed-phase image compared with the in-phase image. The diagnosis of pheochromocytoma was supported by biochemical testing and was proven at histologic analysis after an adrenalectomy.

incidentalomas are metastases, while in oncology patients, the rate is much higher (26%–73%) (1,7). Sites of primary malignancies that most commonly metastasize to the adrenal glands are the lung, bowel, breast, and pancreas (59).

The imaging features of adrenal gland metastases are nonspecific. They usually manifest as indeterminate lesions at nonenhanced CT, without the typical rapid washout seen in adenomas. They also typically do not show signal drop at chemical shift MR imaging. This appearance is no different than that of other malignant tumors, and imaging usually cannot be used to differentiate various malignant tumors of the adrenal glands.

However, special consideration should be given to specific types of metastases that can mimic adenomas. Several malignancies are known to occasionally contain microscopic fat. Metastases from these tumors to the adrenal gland can have the same content of microscopic fat and may show signal drop at chemical shift imaging. These are mostly hepatocellular carcinoma (HCC) (Fig 11), clear cell renal cell carcinoma (RCC) (Fig 12), and, less commonly, granular cell RCC (61,62). HCC and RCC metastases can also show rapid contrast washout and mimic adenomas at adrenal CT (63), which further complicates diagnosis. Therefore, a clinical history of HCC or RCC or a concurrent mass suspected to be HCC or RCC is important for diagnosis and determining the need for follow-up or biopsy. Patients with a known malignancy in whom adrenal metastasis is suspected are the only group for which biopsy is recommended (56).

## Collision Tumors

Collision tumors (defined as the coexistence of two contiguous yet histologically distinct tumors) are an important differential diagnosis when atypical heterogeneous signal drop is seen in the adrenal gland at chemical shift imaging (26). This heterogeneous signal drop occurs when one of the tumors is an adrenal adenoma (64) (Fig 13), but any two tumor types can coexist, both malignant and benign (65). When this is noted, it

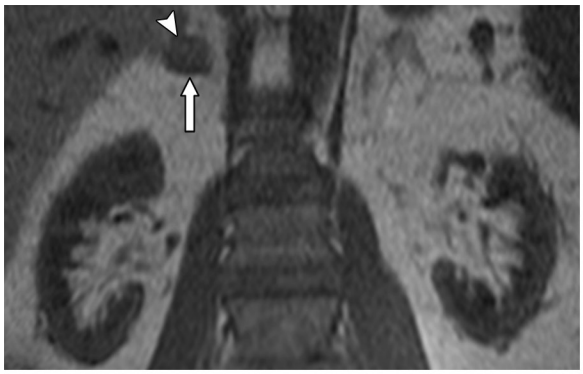

**Figure 9.** Small right adrenal lesion in a 63-year-old man that was detected incidentally at CT for evaluation of hematuria. The lesion measured 39 HU at nonenhanced CT. Coronal in-phase **(a)**, opposed-phase **(b)**, and subtraction **(c)** MR images show a 1.6-cm lesion with a small focus of signal drop in the superior portion (arrowhead) but no signal drop in the remainder of the lesion (arrow). The small focus of microscopic fat is not sufficient for a diagnosis of adenoma. The finding was proven to be a pheochromocytoma after adrenalectomy. The patient was asymptomatic.

**a.**

**b.**

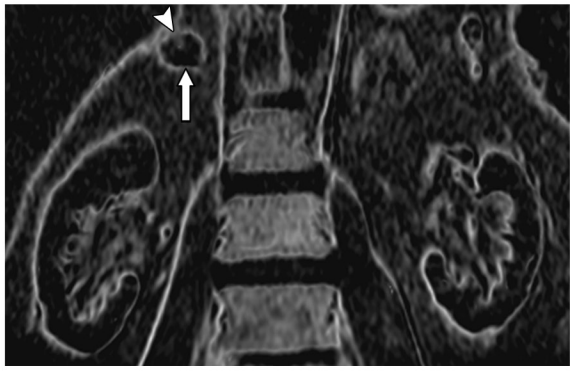

**c.**

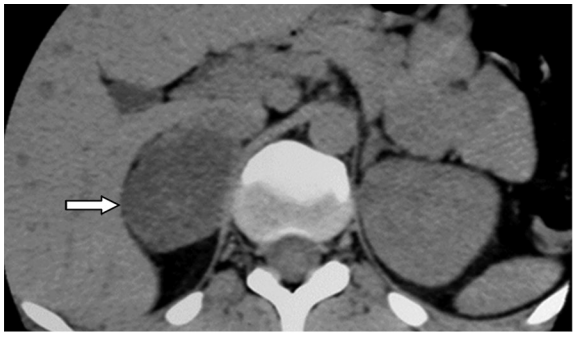

**a.**

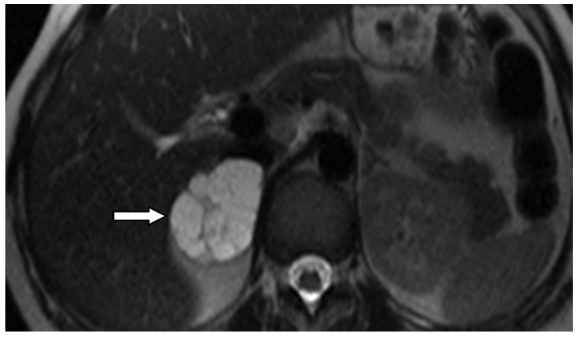

**b.**

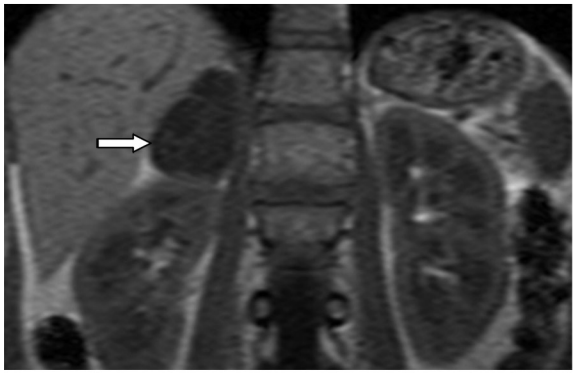

**c.**

**d.**

**Figure 10.** Cystic pheochromocytoma in a 45-year-old man. **(a)** Axial nonenhanced CT image shows a large hypoattenuating lesion measuring 4 HU in the right adrenal gland (arrow). Although this finding is usually sufficient for diagnosis of an adenoma, further evaluation with MR imaging was performed because of the lesion size and clinical suspicion for pheochromocytoma. **(b)** Axial T2-weighted MR image shows the multicystic nature of the lesion (arrow). **(c, d)** Coronal in-phase **(c)** and opposed-phase **(d)** MR images fail to show signal drop characteristic of an adenoma in the lesion (arrow). (Fig 10 adapted and reprinted, with permission, from reference 51.)

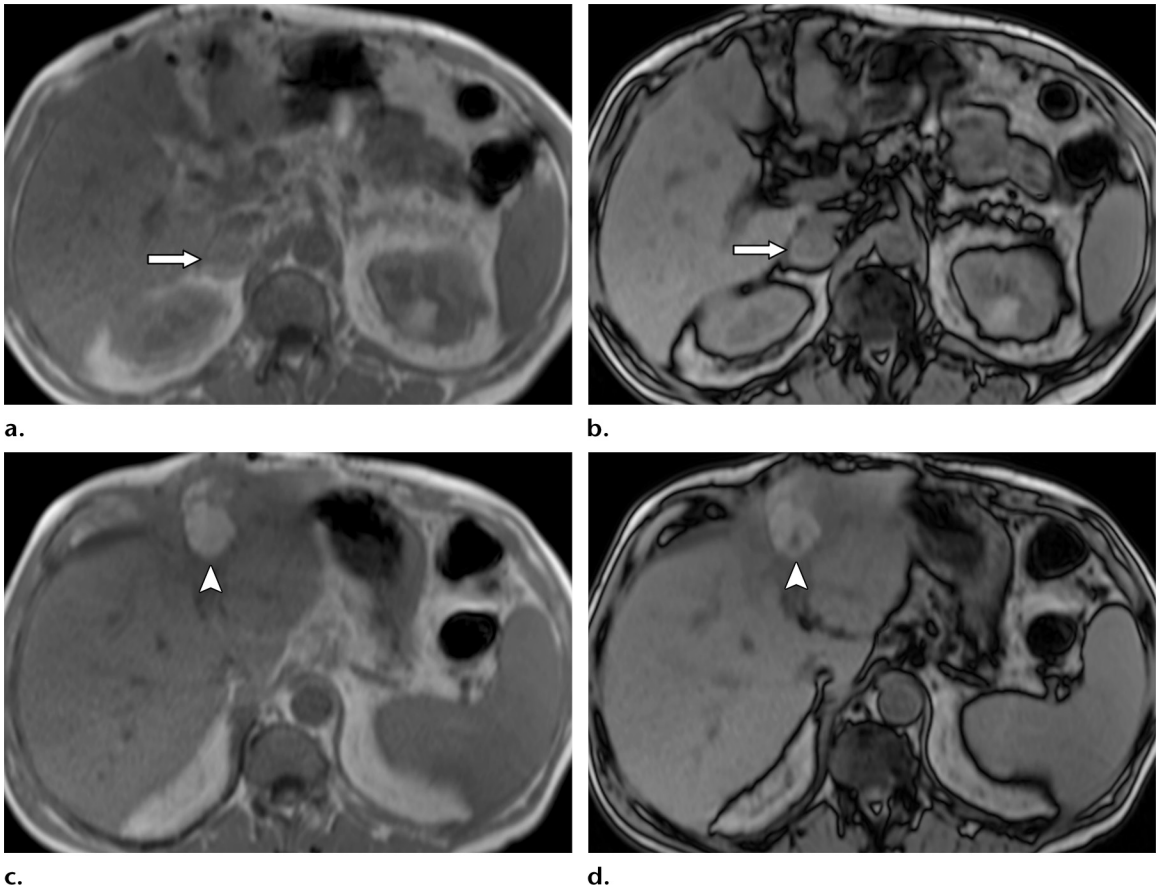


**Figure 11.** New lesion in the right adrenal gland of a 60-year-old man with known HCC. **(a, b)** Axial in-phase **(a)** and opposed-phase **(b)** MR images show signal drop in a right adrenal lesion (arrow). **(c, d)** Axial in-phase **(c)** and opposed-phase **(d)** MR images show a region with signal drop in the primary tumor (arrowhead). The adrenal lesion was proven to be a metastasis from the fat-containing HCC.

is important not to overlook the possible existence of a second tumor type that may necessitate further evaluation or intervention. When a known adenoma changes in size or appearance, especially when a discernible focal lesion is seen within a previously stable lesion and particularly in patients with a known malignancy, a collision tumor should be suspected.

## Myelolipoma

Myelolipomas are benign tumors that contain varying proportions of mature fat tissue and myeloid soft tissue. They usually contain a visible amount of fat, but the spectrum of appearances includes completely fatty lesions and lesions that contain only soft-tissue components (59). They usually are asymptomatic but may enlarge and hemorrhage (26).

The fat seen in myelolipomas is macroscopic fat, and therefore its high T1 signal is suppressed by using routine frequency-selective or inversion-recovery fat-suppression techniques (but not chemical shift imaging). At chemical shift imaging, etching artifact appears in the interface between the macroscopic fat in the myelolipoma and the soft-tissue components of the lesion (Fig 14) or the normal adrenal gland (66). The same artifact can be seen when a myelolipoma is one of the components of a collision tumor. The appearance of etching artifact accentuates the presence of macroscopic fat and can help in diagnosis of myelolipoma, especially in difficult cases.

In small tumors, care must be taken not to mistake the low signal intensity caused by etching artifact for signal drop in the lesion itself, which may lead to erroneous diagnosis of an adenoma. However, the clinical impact of such an error is usually less significant because small adenomas and myelolipomas are generally nonaggressive lesions.

## Hepatic Adrenal Rest Tumor

Hepatic adrenal rest tumors (HARTs) consist of heterotopic aberrant adrenocortical tissue that migrated from the adrenal primordium during embryonic development. They are located in the posterior segment of the right hepatic lobe and are contiguous with the adrenal gland (67), which may cause them to be diagnosed as adrenal tumors. Their imaging appearance may mimic that

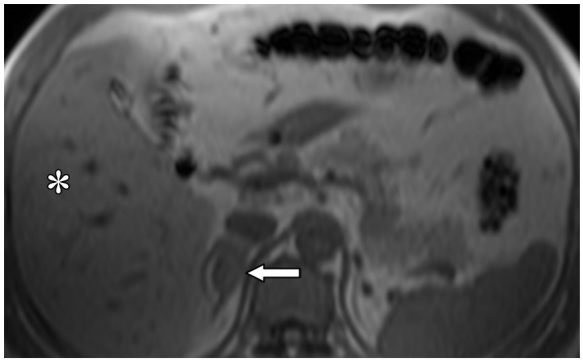

a.

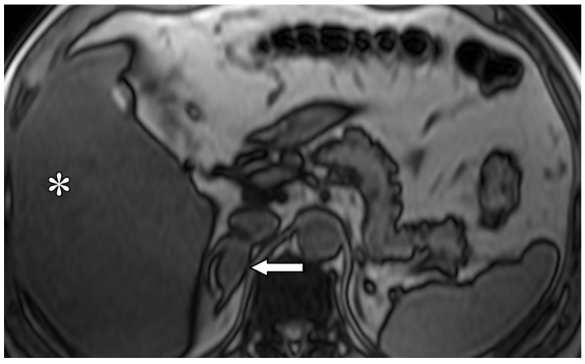

b.

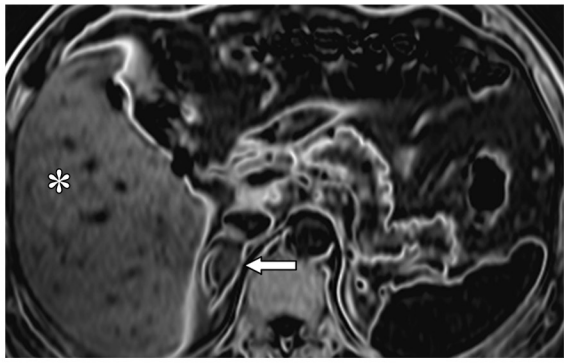

c.

**Figure 12.** Concurrent indeterminate lesion in the right adrenal gland detected at CT in a 45-year-old man with clear cell RCC. MR imaging was performed to evaluate the lesion. **(a, b)** Axial in-phase **(a)** and opposed-phase **(b)** MR images show a 2.9-cm lesion in the right adrenal gland (arrow), but qualitative assessment of signal drop on the opposed-phase image is difficult because signal drop is also seen in the adjacent liver (*) due to fatty infiltration. **(c)** Axial subtraction MR image demonstrates signal drop in the adrenal lesion. Despite the known malignancy, the finding was diagnosed as an adrenal adenoma. Follow-up CT and PET showed increases in size and FDG uptake in the lesion, findings suspicious for a metastasis. Biopsy proved metastatic clear cell RCC.

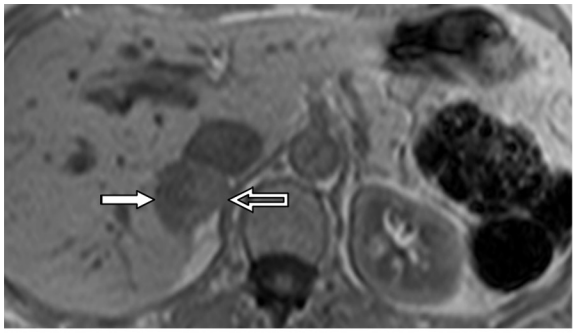

a.

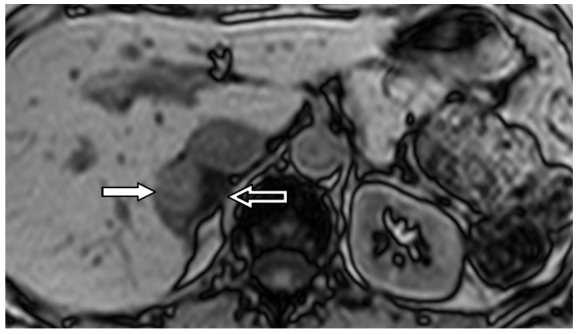

b.

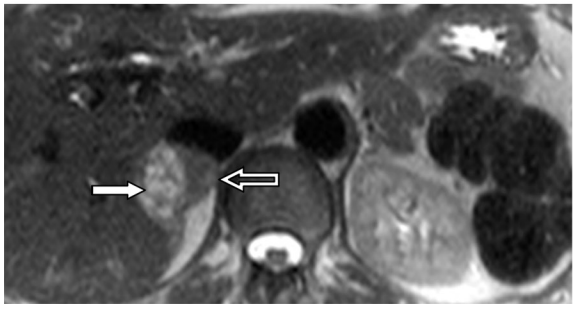

c.

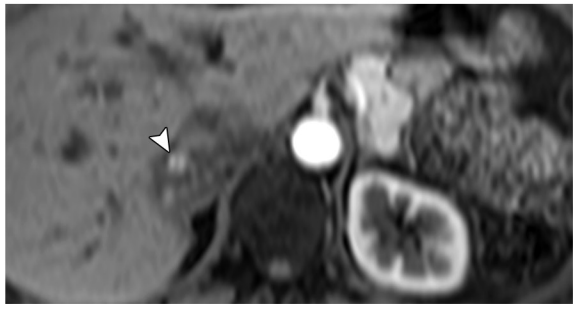

d.

**Figure 13.** Collision tumor in the right adrenal gland of a 64-year-old woman with a known adenoma in the right adrenal gland. Six years after initial diagnosis, CT showed a change in the known adenoma, with the appearance of a slightly more hyperattenuating and partially calcified mass in the lateral aspect. **(a, b)** Axial in-phase **(a)** and opposed-phase **(b)** MR images show a lesion with two different components. The medial component (open arrow in **a–c**) exhibits signal drop consistent with the known adenoma, while the lateral component (solid arrow in **a–c**) does not exhibit signal drop on the opposed-phase image. **(c)** Axial T2-weighted MR image shows that the lateral component has marked hyperintense signal intensity compared with the medial component. **(d)** Contrast-enhanced arterial phase MR image shows nodular enhancement in the lateral component (arrowhead). This appearance is consistent with development of a hemangioma adjacent to the known adenoma, a finding that was proven histologically. (Fig 13 adapted and reprinted, with permission, from reference 64.)

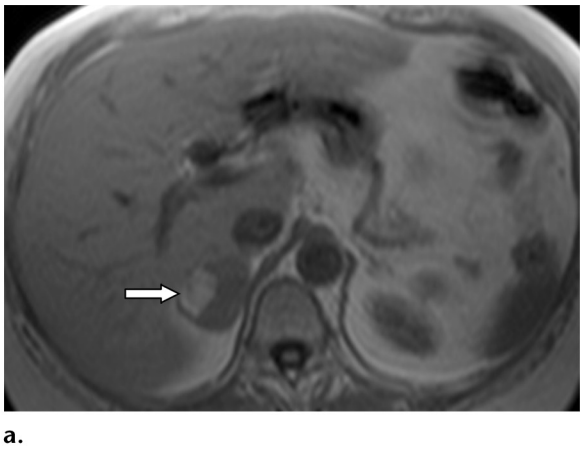

a.

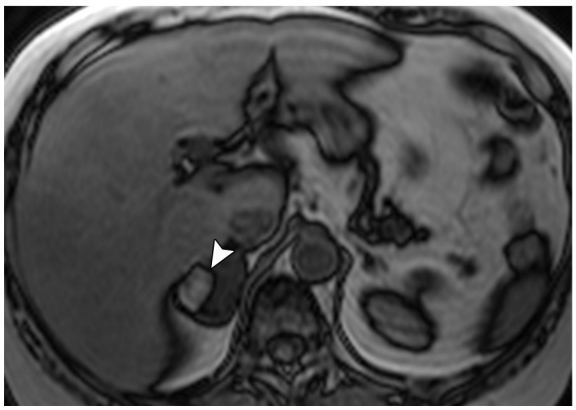

b.

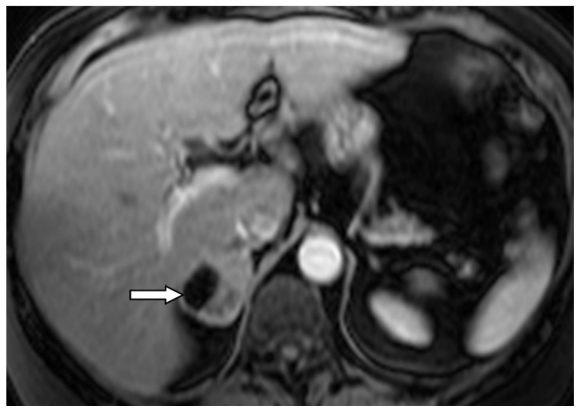

c.

**Figure 14.** Right adrenal lesion in a 61-year-old woman. Axial in-phase **(a)**, opposed-phase **(b)**, and contrast-enhanced fat-suppressed **(c)** MR images demonstrate a lesion with a lateral component (arrow in **a** and **c**) that is markedly T1 hyperintense, does not show signal drop on the opposed-phase image, and shows signal suppression on the frequency-selective image. These findings are consistent with macroscopic fat, and the lesion was diagnosed as a myelolipoma. Note the etching (India ink) artifact (arrowhead in **b**) that delineates the macroscopic fat and separates it from the soft-tissue component.

of HCC, hepatic adenomas, angiomyolipomas, or fat-containing metastases.

HARTs are round and well demarcated. They contain microscopic fat (similar to adenomas) that is visible at chemical shift imaging because they are comprised of adrenal cortical cells, and they often also contain foci of calcification (68). At contrast-enhanced imaging, they are hypervascular because they are supplied by the hepatic artery (Fig 15), which can be helpful to distinguish them from adrenal lesions. Their subcapsular location in the posterior right lobe of the liver, contiguity with the adrenal gland, hepatic arterial blood supply, and signal drop at chemical shift imaging usually enable correct diagnosis.

## Iron Deposition

Iron deposition is the result of iron overload, which can occur locally after hemorrhage (eg, pulmonary hemosiderosis) or systemically as a result of hemolysis, hereditary hemochromatosis, or iatrogenic iron overload from blood transfusions (69). The different forms of iron overload primarily affect different abdominal organs. In hereditary hemochromatosis, iron deposition occurs primarily in parenchymal organs, such as the liver and pancreas. Hemolysis causes deposition of iron primarily in parenchymal organs, mostly the liver and less commonly the kidneys. Iron overload caused by transfusions primarily involves the reticuloendothelial system, and iron deposition is seen in the spleen, liver, and bone marrow (69). Iron deposition in the adrenal glands can occur following blood transfusions (70–72) but has also been reported in hemochromatosis (73).

The paramagnetic effect of iron on T2* accentuates the signal loss normally seen in images with longer echo times (74). At chemical shift imaging, this effect results in signal loss on images acquired using the longer echo time. As explained earlier, at chemical shift imaging, opposed-phase images are optimally acquired early and before in-phase images to avoid naturally occurring T2* effects and thus avoid signal drop that may be wrongfully attributed to fat. With use of this technique, the presence of iron results in an opposite signal change, causing iron-containing tissues to have increased signal intensity on opposed-phase images compared with in-phase images. This paradoxical signal drop, when seen at adrenal MR imaging (Fig 16), should raise suspicion for iron overload and lead to meticulous evaluation of other tissues.

A mimic of iron overload at chemical shift imaging is caused by prolonged use of ferumoxytol (Feraheme, AMAG Pharmaceuticals, Lexington, Mass), which is used to treat iron-deficiency

a.

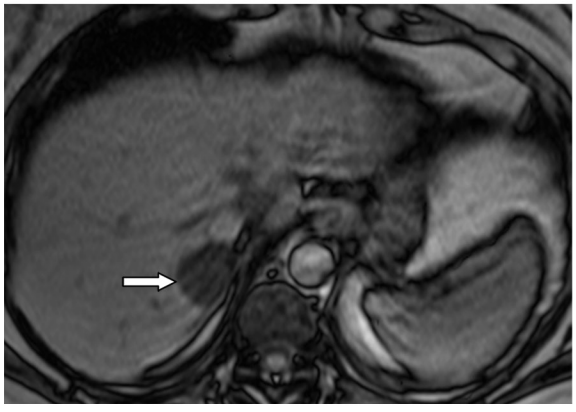

b.

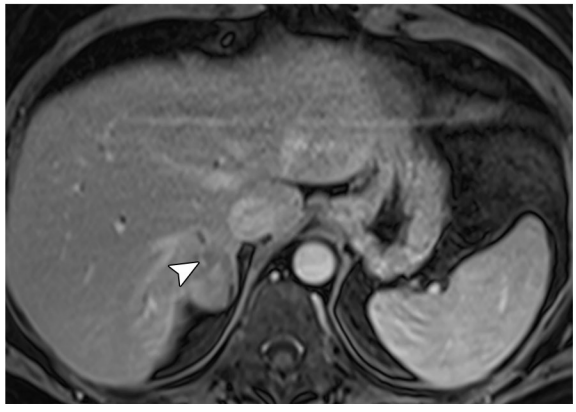

c.

**Figure 15.** HART in a 51-year-old woman. The lesion was detected incidentally at CT and was suspected to be an adrenal malignancy with hepatic spread because it was inseparable from the right adrenal gland. MR imaging was performed for characterization. Axial in-phase **(a)**, opposed-phase **(b)**, and contrast-enhanced **(c)** MR images show a subcapsular lesion (arrow in **a** and **b**) in the posterior aspect of the right hepatic lobe, contiguous with the adrenal gland. The lesion shows signal drop on the opposed-phase image and is supplied by a branch of the hepatic artery (arrowhead in **c**). The lesion was resected and was found to be composed of benign adrenal tissue, a finding consistent with HART.

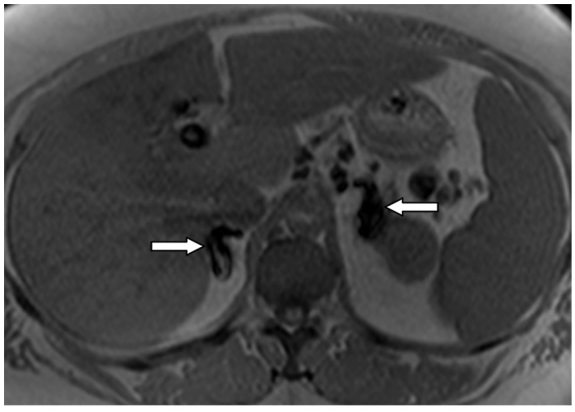

a.

b.

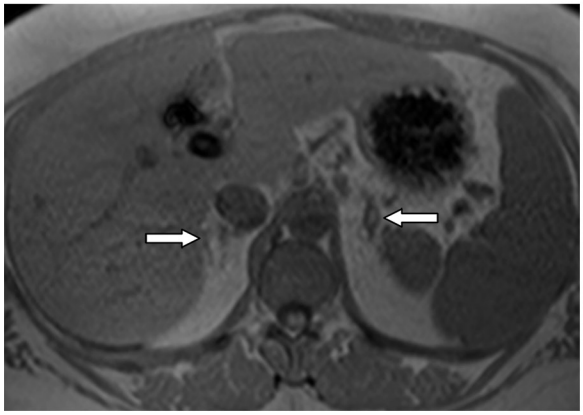

c.

**Figure 16.** Adrenal iron deposition in a 48-year-old woman after multiple blood transfusions. **(a, b)** Axial in-phase **(a)** and opposed-phase **(b)** MR images show lower signal intensity in both adrenal glands (arrows) on the in-phase image than on the opposed-phase image. **(c)** Axial in-phase MR image obtained 6 months earlier shows normal signal intensity in the adrenal glands. The signal drop on the in-phase image in **a** is the result of the T2* effect of iron, which is more pronounced on images with longer echo times, as is the case with in-phase images acquired after opposed-phase images.

anemia. The iron in ferumoxytol is in the form of a superparamagnetic iron oxide. This can cause an appearance similar to that of iron overload at chemical shift imaging despite normal ferritin levels, and it has been debated whether it implies increased iron content in the organs themselves. This effect may be seen in any organ that can be affected by iron deposition and may persist for as long as 3 months (75).

## Conclusion

Chemical shift MR imaging of the adrenal gland is a reliable tool for evaluating the presence of lipid in adrenal lesions to differentiate adrenal adenomas from other lesions. To achieve optimal accuracy and avoid pitfalls, understanding the technique and adhering to technical principles are important. Multiple image analysis methods exist for evaluating adrenal lesions at chemical shift imaging. The preferred method is a matter of personal choice based on the described advantages and disadvantages. Chemical shift imaging is principally used for distinguishing adrenal adenomas from other adrenal lesions, but lesions that are lipid-poor at chemical shift MR imaging may still be adenomas, and rarely other adrenal lesions may mimic adenomas at chemical shift imaging. Therefore, the presence of fat in an adrenal lesion, especially when it is only a small focus of fat, should always be evaluated in an appropriate clinical context.

## References


1. Barzon L, Sonino N, Fallo F, Palu G, Boscaro M. Prevalence and natural history of adrenal incidentalomas. Eur J Endocrinol 2003;149(4):273–285.
2. Bovio S, Cataldi A, Reimondo G, et al. Prevalence of adrenal incidentaloma in a contemporary computerized tomography series. J Endocrinol Invest 2006;29(4):298–302.
3. Davenport C, Liew A, Doherty B, et al. The prevalence of adrenal incidentaloma in routine clinical practice. Endocrine 2011;40(1):80–83.
4. Yamada T, Ishibashi T, Saito H, et al. Adrenal adenomas: relationship between histologic lipid-rich cells and CT attenuation number. Eur J Radiol 2003;48(2):198–202.
5. Korobkin M, Giordano TJ, Brodeur FJ, et al. Adrenal adenomas: relationship between histologic lipid and CT and MR findings. Radiology 1996;200(3):743–747.
6. Mitchell DG, Crovello M, Matteucci T, Petersen RO, Miettinen MM. Benign adrenocortical masses: diagnosis with chemical shift MR imaging. Radiology 1992;185(2):345–351.
7. Blake MA, Cronin CG, Boland GW. Adrenal imaging. AJR Am J Roentgenol 2010;194(6):1450–1460.
8. Pokharel SS, Macura KJ, Kamel IR, Zaheer A. Current MR imaging lipid detection techniques for diagnosis of lesions in the abdomen and pelvis. RadioGraphics 2013;33(3):681–702.
9. Israel GM, Korobkin M, Wang C, Hecht EN, Krinsky GA. Comparison of unenhanced CT and chemical shift MRI in evaluating lipid-rich adrenal adenomas. AJR Am J Roentgenol 2004;183(1):215–219.
10. Hu HH, Kan HE. Quantitative proton MR techniques for measuring fat. NMR Biomed 2013;26(12):1609–1629.
11. de Kerviler E, Leroy-Willig A, Clément O, Frija J. Fat suppression techniques in MRI: an update. Biomed Pharmacother 1998;52(2):69–75.
12. Pereira JM, Sirlin CB, Pinto PS, Casola G. CT and MR imaging of extrahepatic fatty masses of the abdomen and pelvis: techniques, diagnosis, differential diagnosis, and pitfalls. RadioGraphics 2005;25(1):69–85.
13. Soher BJ, Dale BM, Merkle EM. A review of MR physics: 3 T versus 1.5 T. Magn Reson Imaging Clin N Am 2007;15(3):277–290, v.
14. Del Grande F, Santini F, Herzka DA, et al. Fat-suppression techniques for 3-T MR imaging of the musculoskeletal system. RadioGraphics 2014;34(1):217–233.
15. Schieda N, Al Dandan O, Kielar AZ, Flood TA, McInnes MD, Siegelman ES. Pitfalls of adrenal imaging with chemical shift MRI. Clin Radiol 2014;69(11):1186–1197.
16. Schindera ST, Soher BJ, Delong DM, Dale BM, Merkle EM. Effect of echo time pair selection on quantitative analysis for adrenal tumor characterization with in-phase and opposed-phase MR imaging: initial experience. Radiology 2008;248(1):140–147.
17. Merkle EM, Schindera ST. MR imaging of the adrenal glands: 1.5 T versus 3 T. Magn Reson Imaging Clin N Am 2007;15(3):365–372, vii.
18. Marin D, Soher BJ, Dale BM, Boll DT, Youngblood RS, Merkle EM. Characterization of adrenal lesions: comparison of 2D and 3D dual gradient-echo MR imaging at 3 T—preliminary results. Radiology 2010;254(1):179–187.
19. Ramalho M, de Campos RO, Heredia V, et al. Characterization of adrenal lesions with 1.5-T MRI: preliminary observations on comparison of three in-phase and out-of-phase gradient-echo techniques. AJR Am J Roentgenol 2011;197(2):415–423.
20. Heinz-Peer G, Hönigschnabl S, Schneider B, Niederle B, Kaserer K, Lechner G. Characterization of adrenal masses using MR imaging with histopathologic correlation. AJR Am J Roentgenol 1999;173(1):15–22.
21. Korobkin M, Lombardi TJ, Aisen AM, et al. Characterization of adrenal masses with chemical shift and gadolinium-enhanced MR imaging. Radiology 1995;197(2):411–418.
22. Ream JM, Gaing B, Mussi TC, Rosenkrantz AB. Characterization of adrenal lesions at chemical-shift MRI: a direct intraindividual comparison of in- and opposed-phase imaging at 1.5 T and 3 T. AJR Am J Roentgenol 2015;204(3):536–541.
23. Savci G, Yazici Z, Sahin N, Akgöz S, Tuncel E. Value of chemical shift subtraction MRI in characterization of adrenal masses. AJR Am J Roentgenol 2006;186(1):130–135.
24. Haider MA, Ghai S, Jhaveri K, Lockwood G. Chemical shift MR imaging of hyperattenuating (>10 HU) adrenal masses: does it still have a role? Radiology 2004;231(3):711–716.
25. Marin D, Dale BM, Bashir MR, et al. Effectiveness of a three-dimensional dual gradient echo two-point Dixon technique for the characterization of adrenal lesions at 3 Tesla. Eur Radiol 2012;22(1):259–268.
26. Lattin GE Jr, Sturgill ED, Tujo CA, et al. Adrenal tumors and tumor-like conditions in the adult: radiologic-pathologic correlation. RadioGraphics 2014;34(3):805–829.
27. Lee MJ, Hahn PF, Papanicolaou N, et al. Benign and malignant adrenal masses: CT distinction with attenuation coefficients, size, and observer analysis. Radiology 1991;179(2):415–418.
28. Boland GW, Lee MJ, Gazelle GS, Halpern EF, McNicholas MM, Mueller PR. Characterization of adrenal masses using unenhanced CT: an analysis of the CT literature. AJR Am J Roentgenol 1998;171(1):201–204.
29. Blake MA, Kalra MK, Sweeney AT, et al. Distinguishing benign from malignant adrenal masses: multi-detector row CT protocol with 10-minute delay. Radiology 2006;238(2):578–585.
30. Helck A, Hummel N, Meinel FG, Johnson T, Nikolaou K, Graser A. Can single-phase dual-energy CT reliably identify adrenal adenomas? Eur Radiol 2014;24(7):1636–1642.
31. Botsikas D, Triponez F, Boudabbous S, Hansen C, Becker CD, Montet X. Incidental adrenal lesions detected on enhanced abdominal dual-energy CT: can the diagnostic workup be shortened by the implementation of virtual unenhanced images? Eur J Radiol 2014;83(10):1746–1751.
32. Mileto A, Nelson RC, Marin D, Roy Choudhury K, Ho LM. Dual-energy multidetector CT for the characterization of incidental adrenal nodules: diagnostic performance of contrast-enhanced material density analysis. Radiology 2015;274(2):445–454.

33. Foti G, Faccioli N, Manfredi R, Mantovani W, Mucelli RP. Evaluation of relative wash-in ratio of adrenal lesions at early biphasic CT. AJR Am J Roentgenol 2010;194(6):1484–1491.
34. Foti G, Faccioli N, Mantovani W, Malleo G, Manfredi R, Mucelli RP. Incidental adrenal lesions: accuracy of quadriphasic contrast enhanced computed tomography in distinguishing adenomas from nonadenomas. Eur J Radiol 2012;81(8):1742–1750.
35. Caoili EM, Korobkin M, Francis IR, et al. Adrenal masses: characterization with combined unenhanced and delayed enhanced CT. Radiology 2002;222(3):629–633.
36. Koo HJ, Choi HJ, Kim HJ, Kim SO, Cho KS. The value of 15-minute delayed contrast-enhanced CT to differentiate hyperattenuating adrenal masses compared with chemical shift MR imaging. Eur Radiol 2014;24(6):1410–1420.
37. Rodacki K, Ramalho M, Dale BM, et al. Combined chemical shift imaging with early dynamic serial gadolinium-enhanced MRI in the characterization of adrenal lesions. AJR Am J Roentgenol 2014;203(1):99–106.
38. Becker-Weidman D, Kalb B, Mittal PK, et al. Differentiation of lipid-poor adrenal adenomas from non-adenomas with magnetic resonance imaging: utility of dynamic, contrast enhancement and single-shot T2-weighted sequences. Eur J Radiol 2015 Jul 23. [Epub ahead of print]
39. Inan N, Arslan A, Akansel G, Anik Y, Balci NC, Demirci A. Dynamic contrast enhanced MRI in the differential diagnosis of adrenal adenomas and malignant adrenal masses. Eur J Radiol 2008;65(1):154–162.
40. Slapa RZ, Jakubowski W, Januszewicz A, et al. Discriminatory power of MRI for differentiation of adrenal non-adenomas vs adenomas evaluated by means of ROC analysis: can biopsy be obviated? Eur Radiol 2000;10(1):95–104.
41. Miller FH, Wang Y, McCarthy RJ, et al. Utility of diffusion-weighted MRI in characterization of adrenal lesions. AJR Am J Roentgenol 2010;194(2):W179–W185.
42. Gabriel H, Pizzitola V, McComb EN, Wiley E, Miller FH. Adrenal lesions with heterogeneous suppression on chemical shift imaging: clinical implications. J Magn Reson Imaging 2004;19(3):308–316.
43. Newhouse JH, Heffess CS, Wagner BJ, Imray TJ, Adair CF, Davidson AJ. Large degenerated adrenal adenomas: radiologic-pathologic correlation. Radiology 1999;210(2):385–391.
44. Tsushima Y, Takahashi-Taketomi A, Endo K. Diagnostic utility of diffusion-weighted MR imaging and apparent diffusion coefficient value for the diagnosis of adrenal tumors. J Magn Reson Imaging 2009;29(1):112–117.
45. Sandrasegaran K, Patel AA, Ramaswamy R, et al. Characterization of adrenal masses with diffusion-weighted imaging. AJR Am J Roentgenol 2011;197(1):132–138.
46. Halefoglu AM, Altun I, Disli C, Ulusay SM, Ozel BD, Basak M. A prospective study on the utility of diffusion-weighted and quantitative chemical-shift magnetic resonance imaging in the distinction of adrenal adenomas and metastases. J Comput Assist Tomogr 2012;36(4):367–374.
47. Wong KK, Arabi M, Bou-Assaly W, Marzola MC, Rubello D, Gross MD. Evaluation of incidentally discovered adrenal masses with PET and PET/CT. Eur J Radiol 2012;81(3):441–450.
48. Blake MA, Kalra MK, Maher MM, et al. Pheochromocytoma: an imaging chameleon. RadioGraphics 2004;24(suppl 1):S87–S99.
49. Jacques AE, Sahdev A, Sandrasagara M, et al. Adrenal phaeochromocytoma: correlation of MRI appearances with histology and function. Eur Radiol 2008;18(12):2885–2892.
50. Blake MA, Krishnamoorthy SK, Boland GW, et al. Low-density pheochromocytoma on CT: a mimicker of adrenal adenoma. AJR Am J Roentgenol 2003;181(6):1663–1668.
51. Remer EM, Miller FH. Imaging of pheochromocytomas. In: Blake MA, Boland GW, eds. Adrenal imaging. Totowa, NJ: Humana Press, 2009; 1–18.
52. Patel J, Davenport MS, Cohan RH, Caoili EM. Can established CT attenuation and washout criteria for adrenal adenoma accurately exclude pheochromocytoma? AJR Am J Roentgenol 2013;201(1):122–127.
53. Yoon JK, Remer EM, Herts BR. Incidental pheochromocytoma mimicking adrenal adenoma because of rapid contrast enhancement loss. AJR Am J Roentgenol 2006;187(5):1309–1311.
54. Maurea S, Lastoria S, Cuocolo A, Celentano L, Salvatore M. The diagnosis of nonfunctioning pheochromocytoma: the role of I-123 MIBG imaging. Clin Nucl Med 1995;20(1):22–24.
55. Nieman LK. Approach to the patient with an adrenal incidentaloma. J Clin Endocrinol Metab 2010;95(9):4106–4113.
56. Mazzaglia PJ, Monchik JM. Limited value of adrenal biopsy in the evaluation of adrenal neoplasm: a decade of experience. Arch Surg 2009;144(5):465–470.
57. Vanderveen KA, Thompson SM, Callstrom MR, et al. Biopsy of pheochromocytomas and paragangliomas: potential for disaster. Surgery 2009;146(6):1158–1166.
58. Ng L, Libertino JM. Adrenocortical carcinoma: diagnosis, evaluation and treatment. J Urol 2003;169(1):5–11.
59. Elsayes KM, Mukundan G, Narra VR, et al. Adrenal masses: MR imaging features with pathologic correlation. RadioGraphics 2004;24(suppl 1):S73–S86.
60. Egbert N, Elsayes KM, Azar S, Caoili EM. Computed tomography of adrenocortical carcinoma containing macroscopic fat. Cancer Imaging 2010;10:198–200.
61. Sydow BD, Rosen MA, Siegelman ES. Intracellular lipid within metastatic hepatocellular carcinoma of the adrenal gland: a potential diagnostic pitfall of chemical shift imaging of the adrenal gland. AJR Am J Roentgenol 2006;187(5):W550–W551.
62. Woo S, Cho JY, Kim SY, Kim SH. Adrenal adenoma and metastasis from clear cell renal cell carcinoma: can they be differentiated using standard MR techniques? Acta Radiol 2014;55(9):1120–1128.
63. Choi YA, Kim CK, Park BK, Kim B. Evaluation of adrenal metastases from renal cell carcinoma and hepatocellular carcinoma: use of delayed contrast-enhanced CT. Radiology 2013;266(2):514–520.
64. Siddiqi AJ, Miller FH, Kasuganti D, Nikolaidis P. Adrenal hemangioma-adenoma: an exceedingly rare adrenal collision tumor. J Magn Reson Imaging 2009;29(4):949–952.
65. Katabathina VS, Flaherty E, Kaza R, Ojili V, Chintapalli KN, Prasad SR. Adrenal collision tumors and their mimics: multimodality imaging findings. Cancer Imaging 2013;13(4):602–610.
66. Siegelman ES. Adrenal MRI: techniques and clinical applications. J Magn Reson Imaging 2012;36(2):272–285.
67. Baba Y, Beppu T, Imai K, et al. A case of adrenal rest tumor of the liver: radiological imaging and immunohistochemical study of steroidogenic enzymes. Hepatol Res 2008;38(11):1154–1158.
68. Shin YM. Hepatic adrenal rest tumor mimicking hepatocellular carcinoma. Korean J Hepatol 2010;16(3):338–341.
69. Siegelman ES, Mitchell DG, Rubin R, et al. Parenchymal versus reticuloendothelial iron overload in the liver: distinction with MR imaging. Radiology 1991;179(2):361–366.
70. Siegelman ES, Outwater E, Hanau CA, et al. Abdominal iron distribution in sickle cell disease: MR findings in transfusion and nontransfusion dependent patients. J Comput Assist Tomogr 1994;18(1):63–67.
71. Rakow-Penner R, Glader B, Yu H, Vasanawala S. Adrenal and renal corticomedullary junction iron deposition in red cell aplasia. Pediatr Radiol 2010;40(12):1955–1957.
72. Kornreich L, Horev G, Yaniv I, Stein J, Grunebaum M, Zaizov R. Iron overload following bone marrow transplantation in children: MR findings. Pediatr Radiol 1997;27(11):869–872.
73. Machtei A, Klinger G, Shapiro R, Konen O, Sirota L. Clinical and imaging resolution of neonatal hemochromatosis following treatment. Case Rep Crit Care 2014;2014:650916.
74. Merkle EM, Nelson RC. Dual gradient-echo in-phase and opposed-phase hepatic MR imaging: a useful tool for evaluating more than fatty infiltration or fatty sparing. RadioGraphics 2006;26(5):1409–1418.
75. Harman A, Chang KJ, Dupuy D, Rintels P. The long-lasting effect of ferumoxytol on abdominal magnetic resonance imaging. J Comput Assist Tomogr 2014;38(4):571–573.